Grant Agreement no. 640174

PHySIS

Sparse Signal Processing Technologies for HyperSpectral Imaging Systems

INSTRUMENT: Bottom-up space technologies at low TRL
OBJECTIVE: COMPET-06-2014

D2.1 Application Scenarios

Due Date of Deliverable: 30th April 2015

Completion Date of Deliverable: 17th May 2015

Start date of project: 1st March 2015 Duration: 24 months

Lead partner for deliverable: **PLANETEK**

Revision: Final

Project co-funded by the EC within the Horizon 2020 Programme		
Dissemination Level		
PU	Public	✓
PP	Restricted to other programme participants (including the Commission Services)	
RE	Restricted to a group specified by the consortium (including Commission Services)	
CO	Confidential, only for members of the consortium (including Commission Services)	

Document History

Issue Date	Version	Changes Made / Reason for this Issue
17 April 2015	V0.1	Initial draft
23 April 2015	V0.2	Updated ground-based methods
30 April 2015	V0.3	Updated draft
8 May 2015	V0.4	Updated draft
11 May 2015	V0.5	Updated draft
17 May 2015		Final version

Document Main Author(s): **Leonardo Amoruso (PLANETEK)**
Murali Jayapala (IMEC)
Grigorios Tsagkatakis (FORTH)

Document signed off by: **Panagiotis Tsakalides (FORTH)**

Contents

1. Introduction

1.1. Scope

This document is produced in the framework of the PHySIS project and specifically constitutes deliverable D2.1 within WP2.

The general goal of the project is to investigate extensions of compressive signal representations and sparsity-enforcing recovery technologies for the acquisition, compression, restoration, and understanding of hyperspectral data. Specific focus will be put on robust and adaptive mathematical methods able to efficiently recover real-world hyperspectral data, with constraints and noise/perturbation models, as they commonly appear in the fields of Earth observation, astrophysics data processing, and surveillance/security imaging.

WP2 is focusing on the Application Scenarios and System Requirements tasks: it considers the all-around hyperspectral imaging system aspects with specific attention to drivers and constraints gathered from targeted scenarios, in order to define the associated requirements and the system architecture. The specification of system requirements for the application scenarios will follow an iterative process. The detailed scenario descriptions and the associated requirements will be the basis for the work done in the following WPs. This WP will also define and verify mechanisms for achieving and automatically adjusting quality of results at each part of the system. In particular, it will explore and define the metrics that will be used to examine quality of results at each and across stages; and explore and define the interfaces that are required for providing quality feedback among stages.

1.2. Purpose

This document describes the application scenarios identified within the PHySIS project scope. It aims at:

- ✓ specifying application scenarios and describing the operational tasks that cannot be addressed with single-band panchromatic or RGB cameras, in visible or infrared wavelengths;
- ✓ analysing how the operational tasks can be tackled by hyperspectral systems;
- ✓ identifying the hyperspectral design parameters that will play an important role in the overall performance of the system.

This document contributes to the detailed description of the scenarios and to the associated system requirements definition. Both scenarios and requirements will be

updated during project development, according to the results achieved within each of the specific activities (as performed within the other technical work packages).

1.3. Applicable documents

[AD 01] PHySIS_Proposal-SEP-210155336

1.4. Referenced documents

[RD 01] ECSS-E-ST-10C, ECSS Space Engineering – System Engineering general requirements – (issued on 6 March 2009)

[RD 02] ECSS-E-ST-40-06C, ECSS Space Engineering – Software – (issued on 6 March 2009)

[RD 03] CCSDS 311.0-M-1, Reference Architecture For Space Data Systems, September 2008

[RD 04] Space Mission Analysis and Design, James R. Wertz and Wiley J. Larson, eds., Microcosm Press/Springer,1999 (Third Edition)

[RD 05] Hyperspectral Remote Sensing – Principles and Applications M.Borengasser, W.S. Hungate, R. Watkins, CRC Press 2008

[RD 06] Canadian Hyperspectral Spaceborne Mission – Applications and User Requirements K.Staenz, A.Hollinger, 3rd EARSeL Workshop on Imaging Spectroscopy, Herrsching, 13-16 May 2003

[RD 07] Oscar Carrasco, Richard Gomez, Arun Chainani, Willian Roper: Hyperspectral Imaging Applied to Medical Diagnoses and Food Safety. In: Proceedings of SPIE - The International Society for Optical Engineering (Impact Factor: 0.2).08/2003; DOI: 10.1117/12.502589.

[RD 08] D. G. Ferris et al.: Multimodal hyperspectral imaging for the noninvasive diagnosis of cervical Neoplasia, In Journal of Lower Genital Tract Disease. Vol. 5(2), 65–72 (2001).

[RD 09] Robert Koprowski, Sławomir Wilczyński, Zygmunt Wróbel, Sławomir Kasperczyk and Barbara Błońska-Fajfrowska: Automatic method for the dermatological diagnosis of selected hand skin features in hyperspectral imaging. In: BioMedical Engineering OnLine 2014.

[RD 10] Dmitry Yudovsky, Aksone Nouvong, Laurent Pilon: Hyperspectral Imaging in Diabetic Foot Wound Care. In: Journal of Diabetes Science and Technology, Volume 4, Issue 5, September 2010.

[RD 11] Hamed Akbaria, Luma V. Haliga, Hongzheng Zhangb, Dongsheng Wangb, Zhuo Georgia Chenb, and Baowei Feia: Detection of Cancer Metastasis Using a Novel Macroscopic Hyperspectral Method. In: Proc SPIE. 2012; 8317: 831711. doi:10.1117/12.912026.

[RD 12] Guolan Lu, Luma Halig, Dongsheng Wang, Zhuo Georgia Chen, and Baowei Fei: Spectral-Spatial Classification Using Tensor Modeling for Cancer Detection with Hyperspectral Imaging. In: Proc SPIE. 2014 March 21; 9034: 903413–. doi:10.1117/12.2043796.

[RD 13] Hamed Akbari and Yukio Kosugi. Hyperspectral Imaging: a New Modality in Surgery, Recent Advances in Biomedical Engineering, Ganesh R Naik (Ed.), ISBN: 978-953-307-004-9, InTech, (2009) DOI: 10.5772/7478. Available from: http://www.intechopen.com/books/recent-advances-in-biomedical-engineering/hyperspectral-imaging-a-new-modality-in-surgery

[RD 14] Zohaib Khan, Faisal Shafait, and Ajmal Mian: Hyperspectral Imaging for Ink Mismatch Detection. In: 12th International Conference on Document Analysis and Recognition, 2013.

[RD 15] Gerda Edelman , Ton G. van Leeuwen, Maurice C.G. Aalders: Hyperspectral imaging for the age estimation of blood stains at the crime scene. In: Forensic Science Interantional 223 (2012), 72-77.

[RD 16] M.Kubik, Hyperspectral Imaging: A new technique for the non-invasive study of artworks, in Physical techniques in the study of art, archeology and cultural heritage, Vol2, Amsterdam 2007.

[RD 17] R. Padoan, Th.A.G. Steemers, M.E. Klein, B.J. Aalderink, G. de Bruin: Quantitative Hyperspectral Imaging of Historical Documents: Techniques and Applications. In 9th International Conference on NDT of Art, Jerusalem Israel, 25-30 May 2008.

[RD 18] Zarco-Tejada, Pablo J., A. Berjón, R. López-Lozano, J. R. Miller, P. Martín, V. Cachorro, M. R. González, and A. De Frutos. "Assessing vineyard condition with hyperspectral indices: Leaf and canopy reflectance simulation in a row-structured discontinuous canopy." Remote Sensing of Environment 99.3 (2005): 271-287.

[RD 19] S. Livens et.al. ERASEL SIG Imaging Spectroscopy Workshop, 2015

[RD 20] Da-Wen Sun, Hyperspectral Imaging Technology: A Non-Destructive Tool for Food Quality and Safety Evaluation and Inspection, ICEF 2011.

[RD 21] Taoukis, Petros, Nikolaos G. Stoforos, and Vaios T. Karathanos. Advances in Food Process Engineering Research and Applications. Edited by Stavros Yanniotis. Springer, 2013.

[RD 22] L. Liu and M. O. Ngadi .Hyperspectral Imaging for Food Quality and Safety Control, J. Appl. Sci. Technol. (Special Issue No.1): 51-59 (2013)

[RD 23] Fernandez Ramos, Javier, Laurence R. Brewer, Alastair Gorman, and Andrew R. Harvey. "Video-Rate Multispectral Imaging: Application to Microscopy and Macroscopy." In Computational Optical Sensing and Imaging, pp. CW1C-3. Optical Society of America, 2014.

[RD 24] Kester, Robert T., Noah Bedard, Liang Gao, and Tomasz S. Tkaczyk. "Real-time snapshot hyperspectral imaging endoscope." Journal of biomedical optics 16, no. 5 (2011): 056005-056005.

[RD 25] Li, Qingli, Xiaofu He, Yiting Wang, Hongying Liu, Dongrong Xu, and Fangmin Guo. "Review of spectral imaging technology in biomedical engineering: achievements and challenges." Journal of biomedical optics 18, no. 10 (2013): 100901-100901.

[RD 26] Gowen, Aoife A., Yaoze Feng, Edurne Gaston, and Vasilis Valdramidis. "Recent applications of hyperspectral imaging in microbiology." Talanta (2015).

[RD 27] D. Lorente, N. Aleixos, J. Gómez-Sanchis, S. Cubero, O. L. García-Navarrete, and J. Blasco, "Recent Advances and Applications of Hyperspectral Imaging for Fruit and Vegetable Quality Assessment," Food and Bioprocess Technology. May 2012, Volume 5, Issue 4, pp 1121-1142.

[RD 28] E. Bauriegel, and W. B.Herppich, "Hyperspectral and Chlorophyll Fluorescence Imaging for Early Detection of Plant Diseases, with Special Reference to Fusarium spec. Infections on Wheat." In: Agriculture 2014, 4(1), 32-57.

1.5. Definitions, acronyms and abbreviations

ALOS-3:	Advanced Land Observing Satellite-3
ASI:	Agenzia Spaziale Italiana
c.p.s.:	cubes per second
CNES:	Centre National d'études spatiales
CS:	Compressed Sensing
DLR:	Deutsches Zentrum für Luft- und Raumfahrt
ECSS:	European Cooperation for Space Standardization
EnMAP:	Environmental Monitoring and Analysis Program
ESA:	European Space Agency
GSD:	Ground Sampling Distance
HSI:	Hyperspectral Imaging
HYP:	Hyperspectral
HYPXIM:	HYPerspectral-X IMagery
HyspIRI:	Hyperspectral Infrared Imager
JAXA:	Japan Aerospace eXploration Agency
JHM:	Joint Hyperspectral Mission
JPL:	Jet Propulsion Laboratory
LCTF:	Liquid Crystal Tunable Filter
MC:	Matrix Completion
METI:	Ministry of Economy, Trade and Industry
NASA:	National Aeronautics and Space Administration
PAN:	Panchromatic
PHySIS:	Sparse Signal Processing Technologies for HyperSpectral Imaging Systems
PRISMA:	PRecursore IperSpettrale della Missione Applicativa
SNR:	Signal-to-Noise Ratio
SWIR:	Short Wave InfraRed
TBC:	To Be Confirmed
TBD:	To Be Defined

TT&C:	Telemetry, Tracking and Command
VNIR:	Visible and Near InfraRed
USGS:	United States Geological Survey

2. General description

2.1. Product perspective

The rapid development of sophisticated hyperspectral imagers has made the design of dedicated analysis methods a crucial topic. Hyperspectral data can be found in a very wide range of scientific fields ranging from astrophysics (e.g., the ESA/Planck space mission), to satellite monitoring of natural resources (e.g., the ASI/ PRISMA, precursor to the JHM mission, NASA-JPL/HyspIRI, DLR/EnMAP, METI/HISUI on-board JAXA/ALOS-3, CNES/HYPXIM CA), to multi-channel imaging for security and surveillance purposes (e.g., IMEC's hyperspectral imagers). Hyperspectral Imaging (HSI) is becoming an essential tool for distinguishing between physical phenomena with different spectral signatures. HSI is used to solve problems as diverse as the extraction of physically meaningful components (e.g., estimation of astrophysical components in Planck), or to detect anomalies.

The Sparse Signal **P**rocessing Technologies for **Hy**per**S**pectral **I**maging **S**ystems (PHySIS) project is conceived to develop, test, and evaluate novel signal processing technologies for real-time processing of hyperspectral data.

Extracting information requires the joint processing of various kinds of data. This problem turns out to be crucial but challenging as efficient algorithms that take into account the physical structures of such data are lacking. Indeed, the scenes of interest are likely to appear quite distinct in visible (textured, with low dynamics) and infrared (smooth, with very hot spots) bands, and the sensors' sources of noise are generally of different nature. Moreover, they do not share the same resolution. However, these images still represent the same scene; therefore, the joint processing of hyperspectral data is expected to yield enhanced image restoration results. In the field of astrophysics, hyperspectral data generally exhibit heterogeneous characteristics (noise of various origins, different resolutions). Either in astrophysics or in surveillance imaging, extraction of relevant information from hyperspectral data requires the design of adaptive and robust restoration techniques.

Besides, sampling, a key concept of signal acquisition, still follows the long-term paradigm dictated by the classical Shannon-Nyquist theorem, which specifies that to avoid losing information when capturing a signal, we must sample at least twice faster than the signal bandwidth. Nevertheless, in recent years, the theories of Compressed Sensing (CS) and Matrix Completion (MC) reveal that a relatively small number of random incoherent projections of a natural signal can contain most of its salient information. As a result, if a signal is compressible in some orthonormal basis, then a very accurate reconstruction can be obtained from random projections using a small subset of the projection coefficients. When viewed in the framework of data acquisition,

compression/decompression, and restoration, the CS and MC theories provide new insights favouring the design of efficient algorithms for real-time remote sensing applications.

Following acquisition and restoration, hyperspectral data need to be processed for understanding and interpreting their content and the objects being imaged. To achieve this goal, appropriate detection, estimation, and pattern recognition algorithms must be devised, tailored to the peculiarities of each specific application and the characteristics of the hyperspectral data employed. For instance, for low spatial resolution data, such as those mostly captured by hyperspectral sensors on-board space mission satellites, spectral un-mixing must be deployed for image understanding. On the other hand, classification and clustering technologies are more appropriate for the interpretation of high spatial resolution hyperspectral data collected for earth observation, environmental, security, and surveillance applications.

This project aims at implementing and validating the principles of Sparse Representations, Compressed Sensing, and Matrix Completion in the capture, coding, restoration, and interpretation of hyperspectral image and video for power constrained space and remote surveillance systems. Validation will be performed by implementing a prototypal HSI system and demonstrating it in operations.

The overall system for remote sensing and surveillance thus has to be defined with its requirements, its architecture and its specifications: this document is the first step in this definition flow and cares about the identification of relevant scenarios the system will apply to. It provides support to the definition of the whole prototypal system, beginning from its main features, as imaging modes, type and spatial /spectral /temporal density of measurement data (according to each specific scenario), monitoring area and so on. As main driver in system design, the twofold possibility of providing means for HYP data exploitation for public-good usage and for commercial products (or activities), will be carefully considered.

2.2. Spaceborne hyperspectral sensing

2.2.1. Application Scenarios

Although HYP sensors capture massive amounts of high-dimensional data, relevant information usually lies in a low-dimensional space. The aim of the system is to build, and then exploit, recent theoretical and algorithmic developments in sparse signal processing, in the framework of HYP signals.

Possible applications of a HYP acquisition system cover nowadays a wide range, and the possibility to address such a range within the prototypal system is actually un-practical. Furthermore, identifying specific applicative scenarios and introducing them (in this

document) allows to steer analyses and development activities, and to define drivers, constraints and requirements for the final system.

As a first step towards defining appropriate application scenarios, a scout of possible applicative use cases has been performed. To this end, a high-level classification has been made according to the following thematic areas:

- ✓ Terrestrial ecosystems;
- ✓ Aquatic ecosystems;
- ✓ Atmospheric research;
- ✓ Natural resources;
- ✓ Hazards and risks.

Within the scope of these high-level classes, it is then possible to face the following key questions:

- ✓ Climate change impacts and measures
  - Identify consequences of climate change (e.g., global warming) on the state, composition and seasonal cycles of terrestrial and aquatic ecosystems (e.g., coral reefs, boreal forests, etc.);
  - Define strategies on how to reduce the projected climate change and how to implement measures which will be monitored effectively (reducing emissions from deforestation, carbon sequestration in forests and wetlands);
- ✓ Land cover changes and surface processes
  - Quantify the extent and rate of severe land degradation processes (e.g., desertification, ground erosion, salinization, soil acidification) and land use or land cover changes (e.g., deforestation, urbanisation);
  - Detect the consequences of land degradation and land use or land cover changes in view of food security and environmental sustainability;
  - Identify which processes drive land degradation and how efficient are countermeasures;
- ✓ Biodiversity and ecosystem services:
  - Detect ecosystems change over time in their composition and health;
  - Detect the spatial pattern of ecosystem and diversity distributions from local to global scale;
  - Identify how are ecosystem functions and services being altered by human activities or natural causes;
  - Identify harmful consequences on biodiversity to be reduced or prevented;
- ✓ Water availability and quality
  - Detect the quality of inland and coastal water affected by the change of land use and climate, and by management of lakes, rivers and coastal zone;
  - Identify areas that are affected by water scarcity and water quality problems from local to global and from seasonal to decadal scale;
  - Identify how do climate change and human activities, such as intensive agriculture, water demanding industries and high population density, reinforce water scarcity problems;

- ✓ Natural resources management
  - Detect the impact of human activities such as industry, mining, agriculture and others, have on natural resources;
  - Define how can natural resources such as mineral deposits, energy sources (oil, gas), ground water sources and others be explored and managed in a sustainable way;
  - Identify how can environmentally harmful impacts such as water/air pollution, land contamination, mine waste and others be tracked, monitored and managed in order to conserve and sustain natural resource;
- ✓ Geohazard and risk assessment
  - Identify which areas are prone or susceptible to geohazards, such as landslides, floods and others;
  - Identify which land use characteristics affect the vulnerability to geohazards and how can they be mapped and monitored;
  - Identify which areas are to what extent affected and how can this information be provided for short-term coordinated emergency response.

The case studies featured here highlight some of mentioned benefits of HSI. The next Figure sketches the taxonomy of current state-of-art for HYP imaging systems.

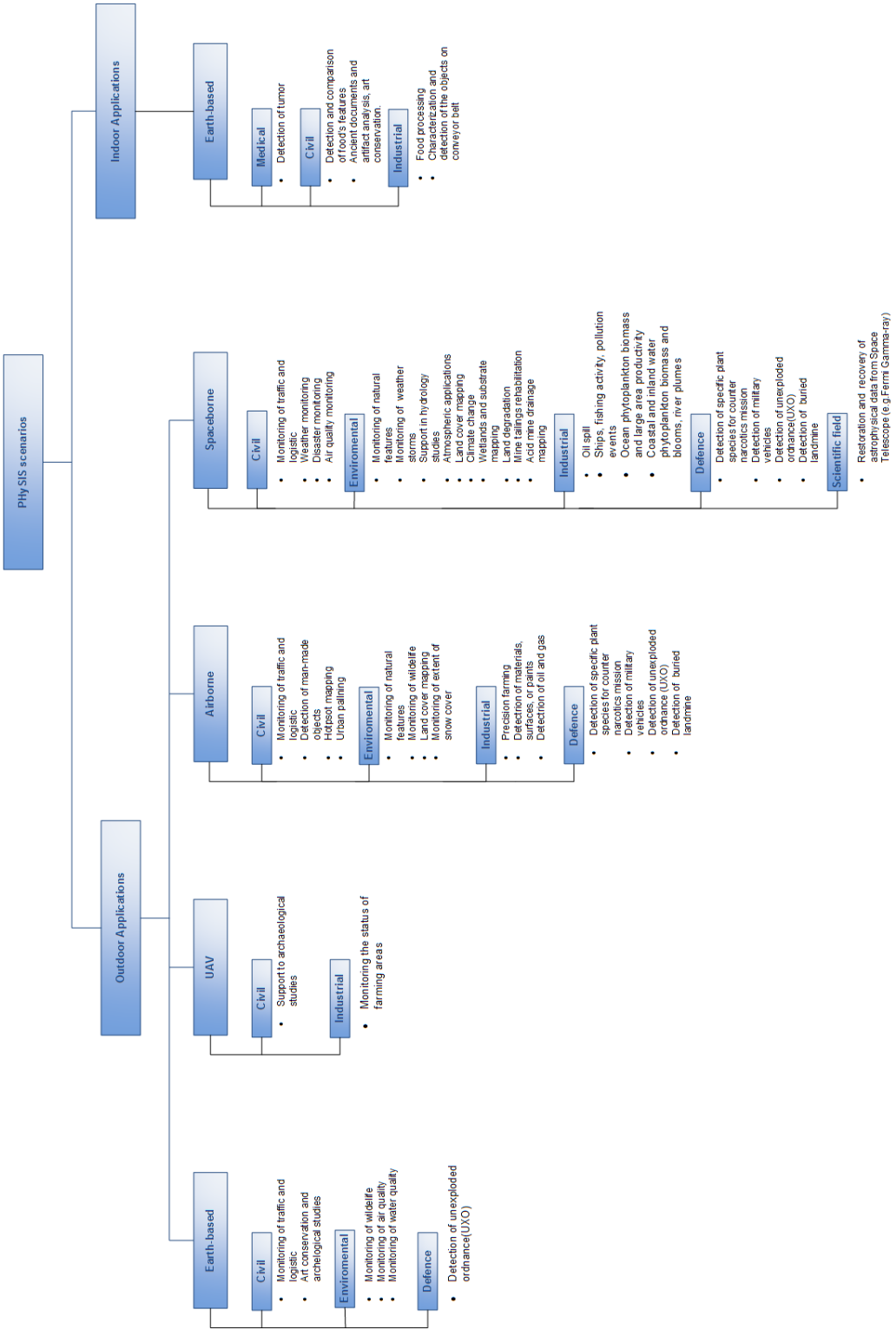

Figure 1: Taxonomy of current state-of-art for hyperspectral imaging systems

Figure 1 clearly depicts how HSI can be exploited as a powerful analysis tool for applications in environment and ecology, aquaculture, forestry, agriculture, and geoscience [RD 05]. A HYP imager's advantage over broadband sensors is its ability to detect molecular absorption and particle scattering signatures of constituents. The finer spectral resolution of a HYP imager allows detection of surface materials, as well as inferences of biological and chemical processes. This capability will also play an important role in addressing issues like sustainability and environment, encompassing the following key areas: agriculture, forestry, geology/soil, coastal/inland waters, and environment.

Therefore, a first assessment on the sensor performance requirements coming from these detected application areas can be defined, resulting in the following most stringent parameters [RD 06]:

- ✓ Specific application area 1: Agriculture
  - spectral resolution in the red-edge region: < 10 nm
  - spectral sampling interval in the VNIR: 5 nm
  - observation frequency: weekly
- ✓ Specific application area 2: Forestry
  - spatial resolution: 1 to 20 m
  - swath width: ≥ 60 km
  - spectral calibration accuracy: < 0.1 nm
- ✓ Specific application area 3: Geology/Soil
  - spectral resolution: < 10 nm
  - peak SNR in SWIR 400:1
    (for a 30 % reflectance target viewed under a 30° solar zenith angle)
  - spectral calibration accuracy: < 0.2 nm
- ✓ Specific application area 4: Coastal/Inland waters
  - spectral coverage: from 370 nm
  - peak SNR >> 100:1 (for a 5 % reflectance target viewed under a 30° solar zenith angle)
  - observation frequency during critical periods: 1 to 3 days
- ✓ Specific application area 5: Environment
  - spectral resolution: < 10 nm
  - spatial resolution: 5 – 20 m
  - peak SNR in the VNIR: > 800:1
    (for a 30 % reflectance target viewed under a 30 ° solar zenith angle)
  - swath width (land cover): ≥ 50 km

Key parameters are Singal-to-Noise Ratio (SNR), spectral resolution, spatial resolution, coverage, and revisit time (specific of spaceborne systems). It should be noted that the retrieval of specific information requires dedicated bands; either located contiguously

over a limited wavelength range or centred at specific wavelength positions. However, to address several applications, the full wavelength coverage is usually required between 400 and 2500 nm.

Information from HYP data today is mostly acquired from airborne platforms, where the spectral and especially the spatial resolution are generally finer than those of satellite systems. Many studies have been carried out with the Airborne Visible/Infrared Imaging Spectrometer (AVIRIS; 10-nm spectral resolution, 20-m spatial resolution, 20-km altitude). Thus, the techniques to extract information are to some extent transferable to the spaceborne domain, though continuous research and development is necessary to bring the information extraction procedures to a mature operational level.

Two main scopes have been defined as the most relevant to be used as our main use cases: i) spaceborne and ii) ground based (terrestrial). The later can be further distinguished in indoor (i.e., in completely characterized and stable acquisition conditions) and outdoor application scenarios.

Of course, these two scopes are distinct, thus they may profit from two different approaches. In fact, the main peculiarity of a spaceborne sensor scenario depends on the strong constraints it has to face as a space system. While in any terrestrial (on the ground or even airborne) application there are degrees of freedom in designing (and dimensioning) the acquisition system, a space system hardly has room for any improvement and so has to deal with limited memory, electrical power, computational power, downlink bandwidth, and so on. Additional constraints are introduced for a spaceborne remote sensing scenario as it will be described in Section 2.2.2.

In contrast to the first case, where we are going to consider “typical” requirements of a HYP mission (even if a specific mission is identified indeed), for a ground-based scenario a specific sensor can be fully identified and characterized (its specification will be reported in Section 2.3).

2.2.2. Onboard operational environment

Technological analyses and developments consider, as a fundamental driver, their applicability in an operative spaceborne scenario. Flexible mini and micro-satellites equipped with high (spatial/spectral) resolution hyperspectral imaging sensors payloads, designed for Earth observation, represent the main use case.

Critical points in the on-board operational environment relate to high data volume handling, for storage, processing, and downlink. A brief description of several hyperspectral /multispectral payloads follows. It includes the characteristics of the sensors, the data handling system (and possible compression approach), and the satellite’s downlink capabilities.

MightySat-II (FTHSI)

MightySat-II is a technology demonstration mission of the US Defense Space Test Program (test of high-risk, high-payoff space system technologies), which was launched in July 2000 and contained the first space-borne HYP sensor, the Fourier Transform Hyperspectral Imager (FTHSI).

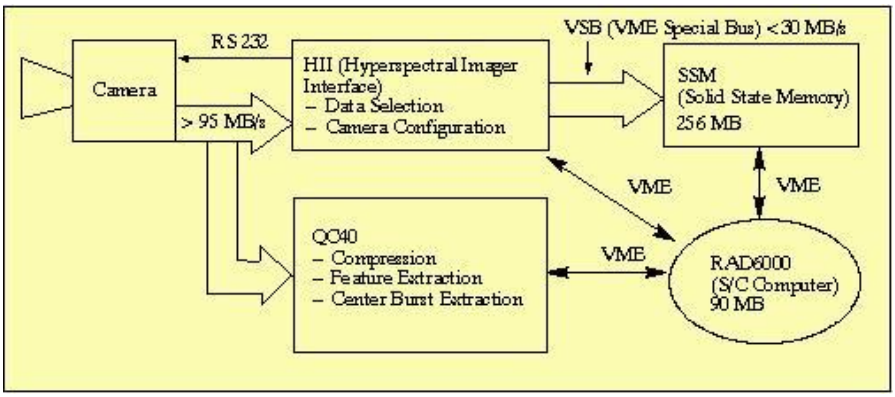

Figure 2: MightySat II block diagram of FTHSI data-handling system
Image credit: Kestrel Corp.

The FTHSI is a visible-near-infrared imaging sensor ranging from 350 – 1050 nm. It is capable to record 256 spectral bands (with 10 bits data quantization) with 1024x1024 spatial pixels (30x30 meters each). Due to the memory restrictions of the data handling system, only 127 bands can be recorded.

The FTHSI was connected to the Quad TMS320C40 Floating Point Signal Processor, i.e. the data handling system of the satellite, which contained 4 microprocessors, a 128Mbyte RAM memory, and 2 Gbit storage. The known operations that were performed on board regarding the compression and processing procedures, were the processing of the raw data (interferogram to image conversion), and their compression (basic encoding for transmission). The consumption of the module was 17W. The down streaming rate was 1Mbit/s.

EO-1 (Hyperion)

EO-1 is a technology demonstration mission in NASA's NMP (New Millennium Program) Earth science program (a Landsat-7 follow-up) with the overall objectives to perform Landsat-like measurements and to explore new remote sensing technologies (instruments, spacecraft, ground segment) that have advanced and enhanced capabilities.

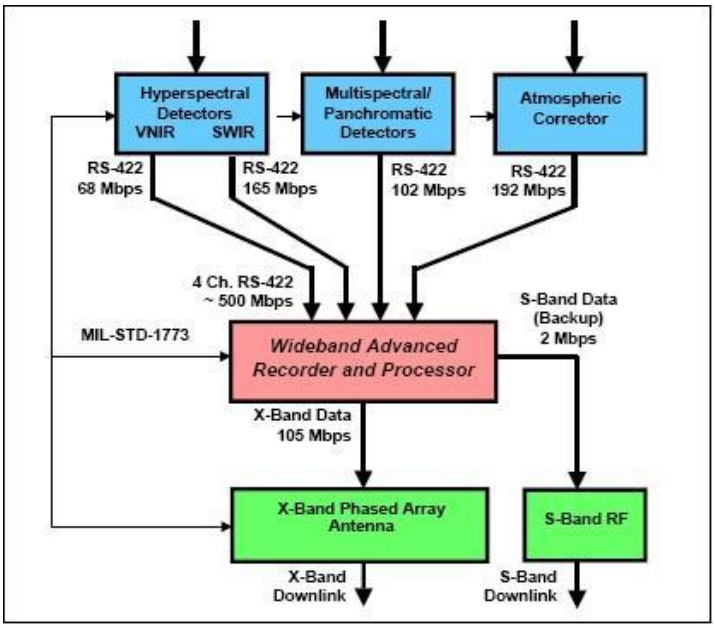

Figure 3: EO-1 data system architecture
Image credit: NASA.

One of the instruments on-board the EO-1 is Hyperion, a pushbroom HYP sensor with two grating imaging spectrometers. A dichroic filter in the sensor reflects the band from 400 to 1000nm to one spectrometer (VNIR) and transmits the band from 900-2,500 nm to the other spectrometer (SWIR). Hyperion records 220 bands (with 12 bits data quantization) in total with 30 meters spatial resolution.

Hyperion is connected to the data handling system of the satellite, named WARP (Wideband Advanced Recorder Processor). WARP is a high-rate solid-state recorder and is used to store the collected data (48 Gbit total storage) and transmit them back to Earth. It contains the Mongoose-V 32-bit processor, which manages the operations of the spacecraft and the post-processing of the data. The WARP system is practically designed to perform basic operations, such as instrument control and image encoding for transmission, but it is not designed to perform complex calculations (e.g. high ratio compression and cloud mapping) optimally. Some experiments were made for image cloud screening, but the hardware limitations prohibited from operationally applying this process. The data downstreaming rate is 105 Mbits/s using the X frequency band.

IMS-1 (HySI)

Indian Microsatellite 1 previously referred as TWSat (Third World Satellite), is a low-cost microsatellite imaging mission of ISRO (Indian Space Research Organization). The overall objective is to provide medium-resolution imagery for developing countries for free.

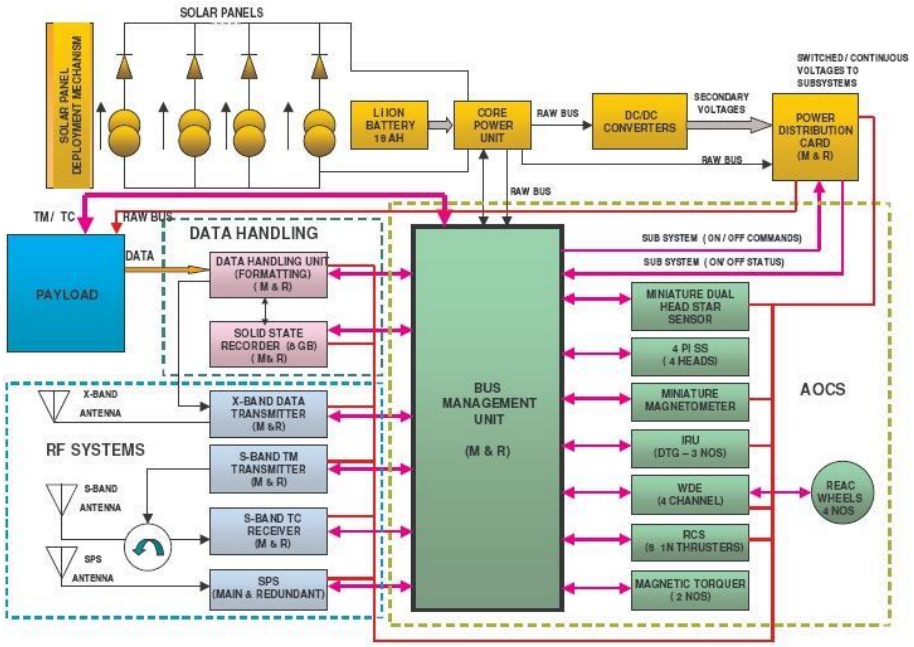

Figure 4: Block diagram for the IMS-1
Image credit: ISRO

One of the instruments onboard the IMS-1 is HySI (Hyperspectral Imager), a pushbroom HYP sensor with 64 fixed spectral bands in the VNIR region. The data quantization of the sensor is 10 bits while the spatial resolution is 550 meters at nadir.

HySI is connected to the data handling system of the satellite [Fig. 3]. This system (BUS Management Unit) is composed of one single printed circuit board and contains all electronics related to data storage, encoding, system controls, etc. The BUS Management Unit compresses the data onboard using the lossy JPEG 2000 algorithm with 3.4:1 compression ratio. Then the data are transmitted back to Earth with an S-Band antenna at 8 Mbit/s rate.

TacSat-3 (ARTEMIS)

TacSat-3 is a follow-up US minisatellite technology demonstration mission within the ORS (Operational Responsive Space) program of DoD, representing a partnership between three military service branches (Naval Research Laboratory, Air Force Research Laboratory, Defense Advanced Research Projects Agency, Army Space and Missile Defense Center, and the USAF Space and Missile Systems Center). TacSat-3 was launched in May 2009. The objective was to last for one year operationally. This objective was met by lasting until 2012.

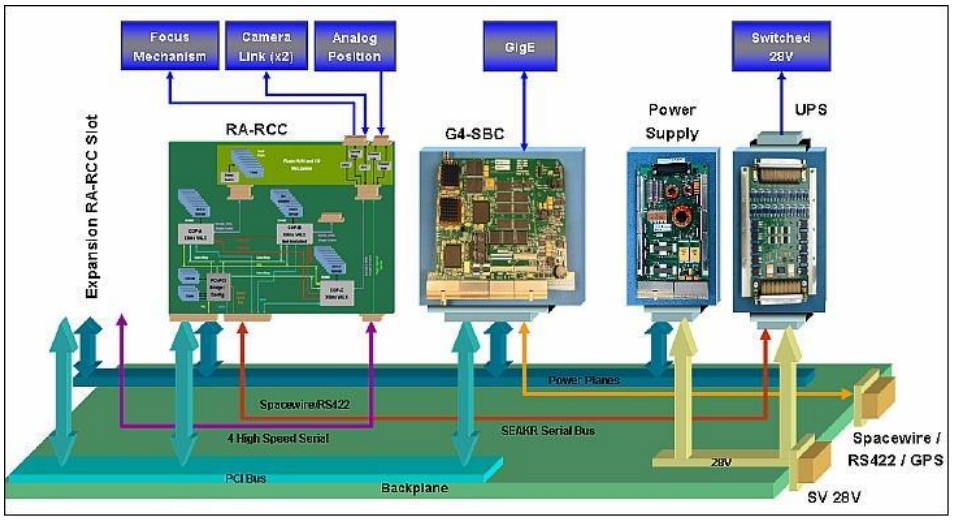

Figure 5: Main components of the ARTEMIS processor architecture
Image Credit: SEAKR Engineering Inc.

One of the instruments onboard the TacSat-3 is ARTEMIS, a pushbroom HYP sensor with 400 continuous spectral bands in the VNIR and SWIR region. The data quantization of the sensor is 10 bits while the spatial resolution is 4 meters.

The system including the ARTEMIS processor is composed of several components, i.e. high performance FPGAs, COTS PowerPC based computer, memory, and communication links. It is used not only for data storage and encoding, but also for on-board tactical target and can either downstream raw HYP images or an RGB image with the identified targets overlaid. It uses the JPEG 2000 algorithm to compress the HYP image. Data are transmitted with an X-Band antenna with rates up to 274 Mbit/s.

Proba-1 (CHRIS)

PROBA is a mini-satellite technology demonstration mission in ESA's General Study Program with the objective to address issues of on-board operational autonomy of a generic platform. It was launched in October 2001.

One of the instruments onboard the PROBA is CHRIS (Compact High Resolution Imaging Spectrometer), a pushbroom HYP sensor with up to 572 spectral bands in the VNIR region. The data quantization of the sensor is 12 bits while the spatial resolution is 34 meters at nadir. Due to memory and processing hardware restrictions only 62 bands are downstreamed back to Earth.

CHRIS is connected to the data handling system of the satellite. This system was designed to integrate in a single redundant unit all the core functions of the spacecraft avionics and to provide sufficiently high-performance computing to support also spacecraft autonomy (i.e. the processing normally performed on-ground has been migrated on-board in the case of PROBA). The Data Management Unit encodes the data

for downstreaming without any specific compression. Data transmission is handled with an S-Band antenna at 1 Mbit/s rate.

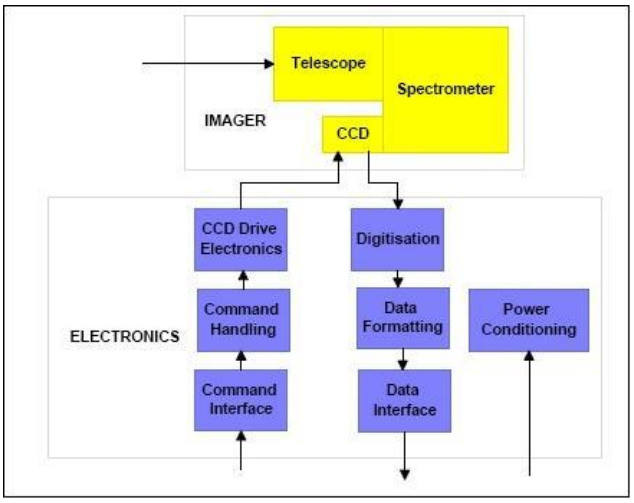

Figure 6: Functional block diagram of CHRIS

Chandrayaan-1 Lunar (HySI, SIR-2, M3)

Chandrayaan-1 is India's first mission to the moon, designed and developed by ISRO (Indian Space Research Organization). It was launched in October 2008. The Chandrayaan-1 satellite contains three HYP instruments: i.) HYP Imager (HySI), ii.) Near Infrared Spectrometer (SIR-2), and iii.) Moon Mineralogy Mapper (M3). Each of the HYP instruments is used for different purposes. The HySI records from 400nm to 930nm with 32 continuous bands, but it could record 256 bands. This restriction originates from hardware and telecommunication bandwidth limits. The SIR-2 is a near infrared spectrometer sensitive from 930nm to 2450nm with 6 nm spectral resolution. This results to 253 spectral bands. The M3 is a NASA funded high spectral resolution imaging spectrometer on-board the Chandrayaan-1 satellite. It records radiation from 700nm to 3000nm with 261 discrete bands. Due to hardware and telecommunication bandwidth restrictions, only 86 are transmitted back to Earth. The scientific data download is performed from the X-band antenna of the satellite at 8Mbit/s.

HIT-SAT (HSC-III)

The Hokkaido Institute of Technology (HIT) developed a technology demonstration satellite HIT-SAT equipped with a HYP imager (HSC-III). It was launched in 2012 with a mission life expectancy of 3 months.

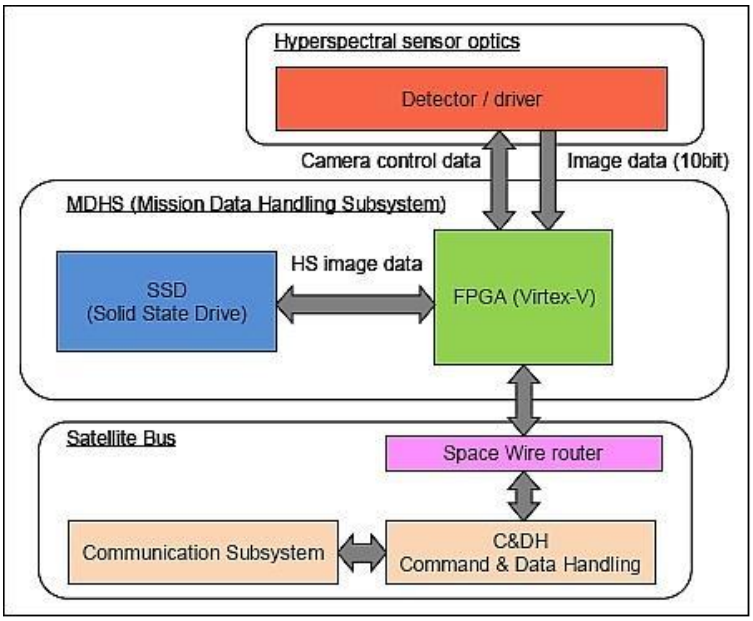

Figure 7: Block diagram of the MDHS including the detector and the satellite bus.

The HSC-III has a spectral range of 400nm-1000nm composed of 138 bands. Due to restrictions in the data handling unit and the downlink bandwidth limitations, only 75 bands are finally transmitted. The spatial resolution of the sensor ranges from 50 to 60 meters.

Figure 7 presents the block diagram of the Mission Data Handling Subsystem. The FPGA is used to process the raw data from the sensor, i.e. select the 75 bands, spatially crop the image, and compress the resulting image (unknown/unpublished compression scheme).

STSat-3 (COMIS)

STSat-3 is a mini-satellite mission of KARI (Korea Aerospace Research Institute), the third experimental microsatellite of the STSat series designated in the long- term plan for Korea's Space Development by the Ministry of Science and Technology. STSat-3 was launched in 2013. COMIS is the secondary payload, an imaging spectrometer, which was inspired by the success of CHRIS, developed for the PROBA-1 mission of ESA. COMIS takes HYP images of 27 m GSD (Ground Sampling Distance) over a 28 km swath width. It is able to record up to 120 bands ranging from 400nm to 1050nm, but the maximum number of transmitted bands is 64.The CDS (Command & Data Handling Subsystem) is composed of the OBC (On-Board Computer), MMU (Mass Memory Unit), and TCTM (TeleCommand & TeleMetry Unit). The CDS is an on-orbit reconfigurable subsystem which is based on the Leon3-FT (Fault Tolerant) processor by uploading FPGA code and flight software code. This feature permits to modify, upgrade and even change the system during the mission. It includes use of TMR (Triple Module Redundancy) technology for SEU (Single Event Upset) mitigation and implementation of the

configuration memory scrubbing algorithm to protect the FPGA, and use of the EDAC (Error Detection and Correction) algorithm for memory protection. The FPGA then communicates with the rest of the satellite systems using the standard protocol of the Space Wire Router. No compression scheme is specified besides the spectral sub-setting of the bands.

EnMAP (HSI)

The Environmental Mapping and Analysis Program (EnMAP) is a German HYP satellite mission, a co-operation between the German Research Centre for Geosciences (GFZ), Kayser-Threde, OHB and the Space Administration Division of the German Aerospace Center (DLR) that aims at monitoring and characterising the Earth's environment on a global scale. The envisaged launch of the EnMAP satellite will happen in 2018 and the mission lifetime is 5 years.

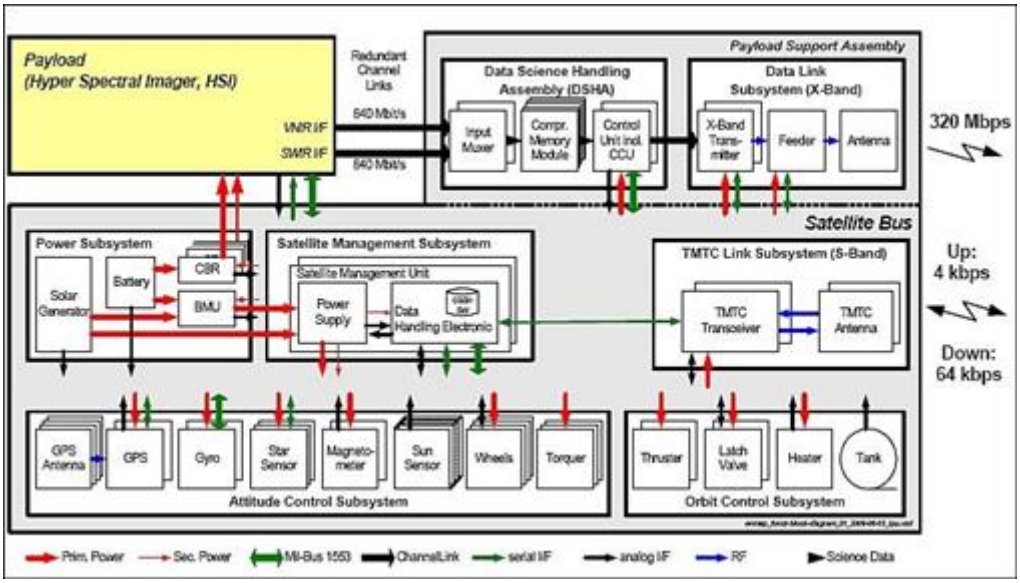

Figure 8: Block diagram of the EnMAP's onboard data handling system including the detector and the satellite bus.

The HYP sensor (HSI Instument) is an imaging pushbroom with a broad spectral range: from 420 nm to 1000 nm, with a mean band width of 6.5 nm (VNIR), and from 900 nm to 2450 nm with a band width of 10 nm (SWIR). So it provides high radiometric resolution and stability in both spectral ranges, on the 89 VNIR and 155 SWIR bands. The designed swath is 30km wide at a spatial resolution of 30 m x 30 m and can be steered to point angles till to 30° off-nadir, for a fast target revisit (4 days). On-board memory is 512 Gbit large and allows to acquire 1,000 km swath length per orbit and a total of 5,000 km per day, having radiometric resolution equal to 14 bits.

ALOS-3 (HSUI)

The Advanced Land Observing Satellite-3 (ALOS-3) is a JAXA optical satellite mission which carries an optical sensor complement comprised of the optical instruments PRISM-2 (Panchromatic Remote-sensing Instrument for Stereo Mapping) and HISUI (Hyperspectral Imager Suite), featuring panchromatic and multispectral imaging capability as well as HYP imaging capability. HISUI comprises two elements: a multispectral imager, also referred to as MSS (Multispectral Sensor), with excellent spatial resolution and swath width, and a HYP imager, also referred to as HSS (Hyperspectral Sensor), with a high identification capability thanks to a high wavelength resolution (total of 185 bands).

SENTINEL-2 (MSI)

The Sentinel-2 mission is based on a constellation of two satellites (A and B units), within the Copernicus program, jointly implemented by the European Commission and ESA for global land observation (data on vegetation, soil and water cover for land, inland waterways and coastal areas, atmospheric absorption and distortion data corrections). Each satellite provides high resolution imaging and high revisit capability, in order to provide enhanced continuity of the data so far provided by SPOT-5 and Landsat-7. The MultiSpectral Imager (MSI) instrument is based on the pushbroom observation concept. MSI features 13 spectral bands spanning from the VNIR (Visible and Near Infrared) to the SWIR (Short-Wave Infrared), featuring 4 spectral bands at 10 m, 6 bands at 20 m and 3 bands at 60 m spatial sampling distance (SSD). The observation data are digitized on 12 bit and the average observation time per orbit is 16.3 minutes, while the peak value is 31 minutes (duty cycle of 16-31%). The expected data rate is of 490 Mbps (after compression). One of the key technologies exploited by Sentinel-2 is the Mass Memory & Formatting Unit (MMFU), i.e. the first European Mass Memory System based on NAND-Flash Storage Technology. It is based on a 2.4 Tbit solid state mass memory and the payload data downlink is performed at a data rate of 560 Mbit/s in X-band with 4 core X-band ground stations for full mission data recovery by the Copernicus PDGS (Payload Data Ground System).

LANDSAT-8 (OLI)

Landsat-8 is an American Earth observation satellite designed in a collaboration between NASA and the United States Geological Survey (USGS) and launched in 2013. Its swath width equals to 180 km and a GSD of 15 and 30 m for panchromatic and multispectral sensor, respectively. About 400 scenes are obtained every day which amounts to about 390 GB, which are stored in a 500 GB data recorder. An X-band downlink system with a performance of 384 Mbps is used at three ground stations. The total amount of downlink time is about 98 minutes/day. Moreover, many ground stations take part in receiving Landsat-8 data under the contract with USGS. In

summary, Landsat-8 provides moderate spatial resolution data operationally, which is suitable to downlink all the land observation data using the ground stations located at polar region directly. In particular, the Operational Land Imager (OLI) design features a multispectral imager with a pushbroom architecture. The OLI acquires ~400 scenes per day in six VNIR and three SWIR bands (covering a spectral range from 443 nm to 2300 nm), all at 12 bit radiometric resolution. In addition to these bands there will be a tenth band consisting of covered SWIR detectors, referred to as the 'blind' band, that will be used to estimate variation in detector bias during nominal Earth image acquisitions.

Table 1 summarizes compression capabilities, number of bands that can be acquired by each sensor, while the "transmitted bands" corresponds the number of bands that actually are down streamed back to Earth.

Table 1: Hyperspectral satellites characteristics

Parameter	Bands	Transmitted	Quantization	Data Compression	Type	Algorithm	Compression Dedicated	Type of Hardware
MightySat-II	256	127	10	NO	N/A	N/A	NO	N/A
EO-1	220	220	12	NO	N/A	N/A	NO	N/A
IMS-1	64	64	10	YES	Lossy	JPEG2000	NO	N/A
TacSat-3	400	400	10	YES	Lossy	JPEG2000	YES	FPGA
Proba-1	572	62	12	YES	Lossy	Spectral subsets	NO	N/A
Chandrayan-1 Lunar HySI	256	32	12	YES	Lossy and Lossless	Not specified. Lossless compression ratio up to 1.8	NO	N/A
Chandrayan-1 Lunar SIR-2	253	253						
Chandrayan-1 Lunar M^3	261	86						
HIT-SAT	138	75	10	YES	Unknown	Unknown	YES	FPGA
STSat-3	120	64	16	YES	Lossy	Spectral subsets	YES	LEON3 + FPGA
EnMAP	244	244	14	YES	Lossless	CCSDS-122.0	YES	FPGA
ALOS-3	189	189	12	YES	Lossless	Spectral Correlation	YES	FPGA
Sentinel-2	13	13	12	YES	Lossy	Wavelet-based	N/A	N/A
Landsat 8	9	9	12	YES	Lossless	Rice	YES	ASIC

2.3. Ground-based hyperspectral sensing

This section provides an overview of the various applications of HSI in terrestrial and in general ground-based applications. Figure 9 provides a visual illustration of some of these applications.

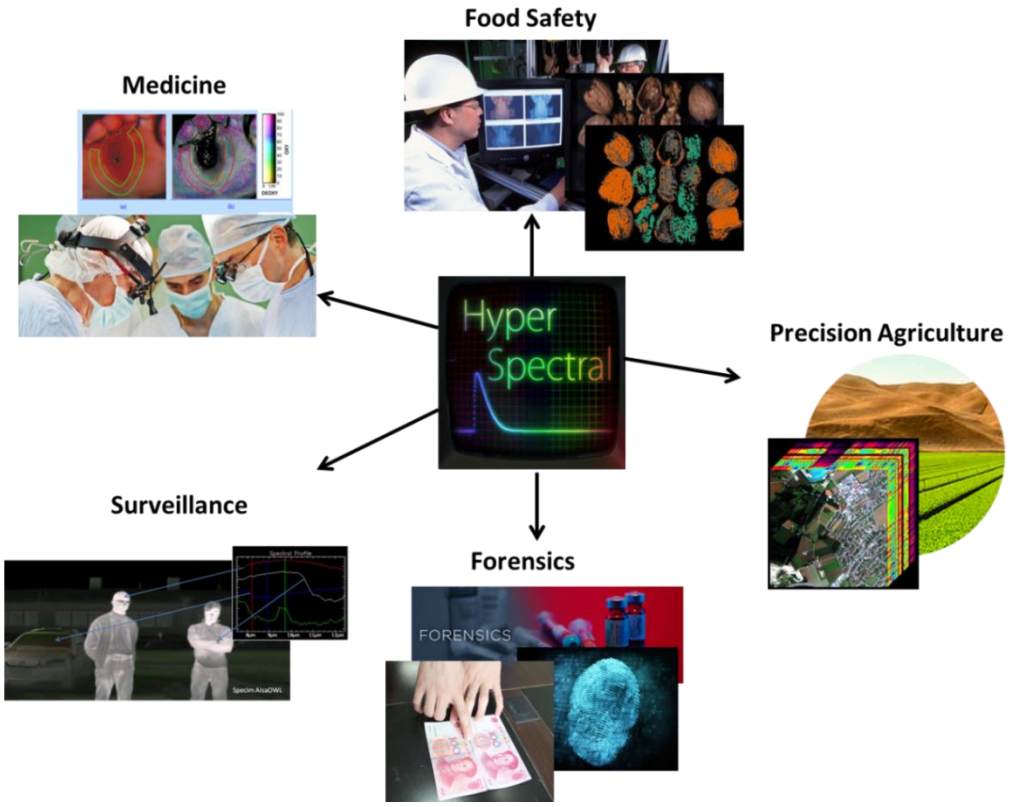

Figure 9: Outline of ground-based applications of HSI

2.3.1. HSI for precision agriculture

HSI for early detection of plant diseases

This section outlines state-of-the-art spectral approaches concerning plant diseases, with special interest to *Fusarium* head blight (FHB) in cereal production. FHB cereal infection is a significant disease resulting not only in the reduction of yield, and the degradation of milling quality, but also in the contamination of grains with mycotoxins. HSI are proved to be significant tools in the early detection of the specific plant diseases. Table 2 summarizes related approaches that operate on specific spectral bands and target the detection of significant ingredients, such as protein detection, changes in carbohydrates etc. For more information regarding the Fusarium infections on wheat and the application of HSI for early detection, refer to [RD 27].

Table 2: HSI applications on selected plant-pathogen systems

Plant Plant-Pathogen system	Relevant Spectral Lines	Targets/Method	References
Triticum aestivum-Fusarium	550–560 nm 665–675 nm	detection of carotenoids and chlorophylls	Bauriegel et.al (*2010*)
Beta vulgaris—Cercospora beticola, Erysiphe betae* and *Uromyces betae	10 optimal wavelengths between 450–1650 nm		Nieuwenhuizen, et.al (*2010*)
***Zea mays—Fusarium verticilloides* (grains)**	1960 and 2100 nm for infected; 1450, 2300 and 2350 nm for non-infected grains	changes of carbohydrate and protein contents	Williams, et.al (*2010*)
***Triticum aestivum—Fusarium* (grains)**	1182 and 1242 nm		Delwiche, et.al (*2003*)
***Triticum aestivum—Fusarium* (grains)**	1425 to 1440 nm and 1915 to 1930 nm	DON estimation changes of carbohydrates, proteins and lipid contents	Peiris, et.al (*2009*)
***Triticum aestivum—Fusarium* (grains)**	1204, 1365 and 1700 nm	DON estimation changes of carbohydrates, proteins and lipid contents	Dowell,et.al (1999)
***Triticum aestivum—Penecillium* spp. and *Aspergillus* species (grains)**	1284, 1316, 1347 nm	changes of carbohydrates, proteins and lipid contents	Singh, et.al (*2007*)
Triticum aestivum—Fusarium Culmorum	430–1750 nm	method: PLS	Polder, et.al (*2005*)
Triticum aestivum—Drechslera tritici-repenti	550–750 nm	methods: PCA, FVBA	Muhammed, et.al (*2003*)
Beta vulgaris—Heterodera	400–1000 nm	methods: SVI, SAM	Hillnhuetter, et.al (*2012*)

schachtii* and *Rhizoctonia solani			
***Triticum aestivum*—*Fusarium* spp**	670 ± 22, 800 ± 65 nm		Dammer, et.al (*2011*)
Triticum aestivum*—*Fusarium	bands in R, MIR and NIR	changes of chlorophyll and carotenoids	Laguette, et.al (2004)

Hyperspectral imaging for precision agriculture using Drones/UAV

Agriculture is an old but yet a very large and diverse industry that is facing a number of challenges. One of them is to increase the productivity drastically. For example, there are reports claiming that farmers need to produce more food to keep up in the next 50 years than what has been produced in the last 10,000 years. There is also a pressure to reduce economic and ecological footprint, especially with respect to usage of chemicals and water in farming and agriculture. To address these challenges, the trend is to go towards precision agriculture, where the aim is to use technological solutions to drastically improve the productivity and reduce/improve the ecological footprint. HYP technology, especially when combined with drones or UAVs, raises as a promising technology solution to address these challenges. Currently, there are several companies (e.g., Parrot/Sensefly/Pix4D[1][2], Gamaya[3]) which are using drones mapping the agricultural fields, and surveying low altitudes using multispectral sensors instead of traditional earth observation techniques using satellites.

Worldwide, great effort is spent on agricultural field experiments. The effects of fertilizers, cultivation methods, treatments and seed varieties are tested through comparative trials on adjacent plots. The results are of immediate interest to farmers. Field trials are also vital to gather important scientific information, such as to assess the performance of new traits, and to gather environmental safety data required by regulatory authorities to evaluate commercial product approvals. Typical spectral ranges of interest in precision agriculture are to some extent summarized in Figure 10. In addition, there is a large number of vegetation indices, for instance, the NDVI index using one band in NIR and another band is visible spectrum, especially in the VISNIR range (400-1000nm) that is of significant interest targeting growth of maize, corn, trees/shurbs, and wheat [RD 18].

[1] https://www.sensefly.com/home.html

[2] https://pix4d.com/

[3] http://gamaya.com/

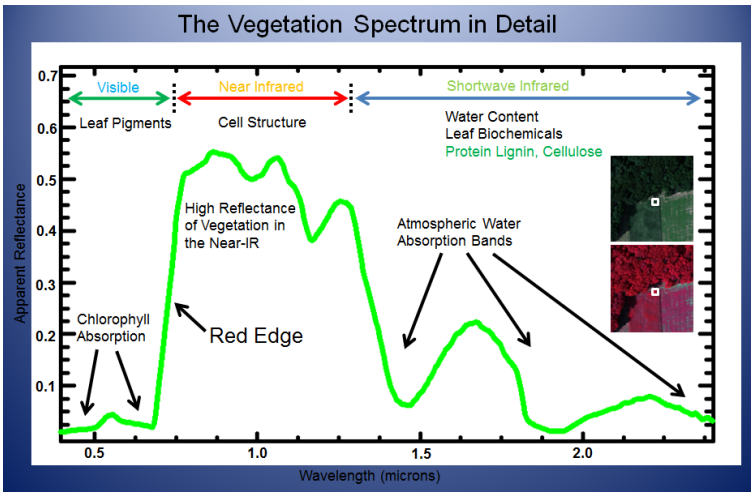

Figure 10: The vegetation spectrum in detail

Requirements for HSI in this context:

- Compact & light weight < 100gr
- VISNIR: 400-1000nm
- Bands < 100 (typically open, there is not yet a convergence on specific number of bands)
- Daylight/natural illumination
- Snapshot & Linescan/pushbroom (both are acceptable)
- Typically on-board data capture, processing after flight of UAV/Drone. The trend is to generate some initial results to feed to the operator to give some real-time information.

2.3.2. Hyperspectral imaging for food quality grading

Over the years, optical sensing technologies have been investigated as potential tools for non-destructive evaluation and inspection for food quality and safety. Conventional imaging systems are typically coupled with computer vision (also known as machine vision) algorithms for detecting on and under the surface features. These systems typically consist of a light source along with an array of spectral detectors, where the light source provides illumination to the sample and the array detectors capture mixed spectral contents from the sample. Spatial information of the sample is obtained in the form of monochromatic or colour images, thus conventional imaging systems typically employ colour, shape, size and surface texture for the evaluation of food products and for the detection of surface defects during food inspection. Unfortunately, typical architectures cannot identify or detect chemical properties or characteristics of food products. HYP imaging (or imaging spectroscopy) has emerged as a technology with great potential for effective and non-destructive quality and safety evaluation and inspection in the area of food processing [RD 20].

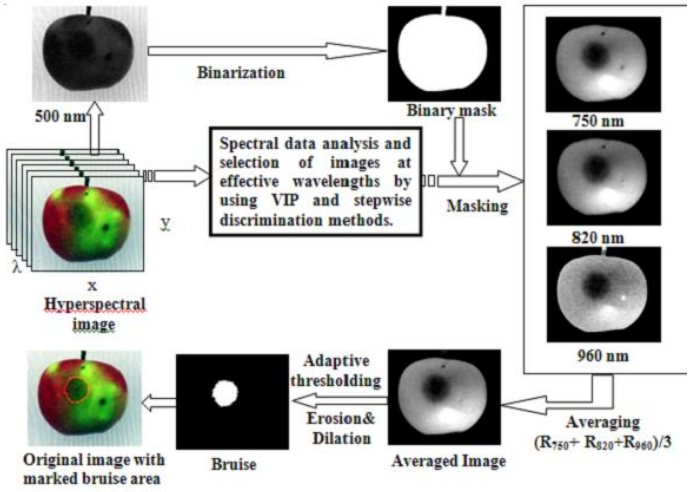

Figure 11: Hyperspectral imaging for food processing

Many approaches and applications have demonstrated the potential of HSI in the food industry. These applications include i) meat quality assessment, ii) automated poultry carcass inspection, iii) quality evaluation of fish, iv) bruise detection of apples, v) quality analysis and grading of citrus fruits, vi) bruise detection of strawberry, vii) visualization of sugar distribution of melons, viii) measuring ripening of tomatoes, ix) defect detection of pickling cucumber, and x) classification of wheat kernels. Most of the analysis can be readily performed in the spectral range of 400-1000nm [RD 20, RD 21]. Figure 11 presents an example of bruise detection in apples [RD 20].

Depending on the object to be assessed and the technique of image acquisition, the specific configuration of the HSI system will differ with respect to hardware and software components. The majority of hardware platforms for HSI however, share some common basic components as shown in Figure 12; namely a light source to provide illumination (usually produced by halogen lamps); HYP detector which obtains both spectral and spatial resolution simultaneously; an objective lens to adjust the range of light acquisition; an objective table fixed to a conveyer belt to hold and transport the sample; and a computer to compose, store, and analyze the three-dimensional hypercube in real-time [RD 22].

Requirements for HSI in this context:

- VNIR: 400-1000nm
- Bands < 100 (typically open, there is not yet a convergence on specific number of bands)
- Controlled illumination (using halogen lamps/LEDs)
- Snapshot & Linescan/pushbroom (both are acceptable)
- High-speed: short intervals from data capture to decision. To match with high speed of conveyor belt speeds (~ few cm/s to even up to 2-3m/s)

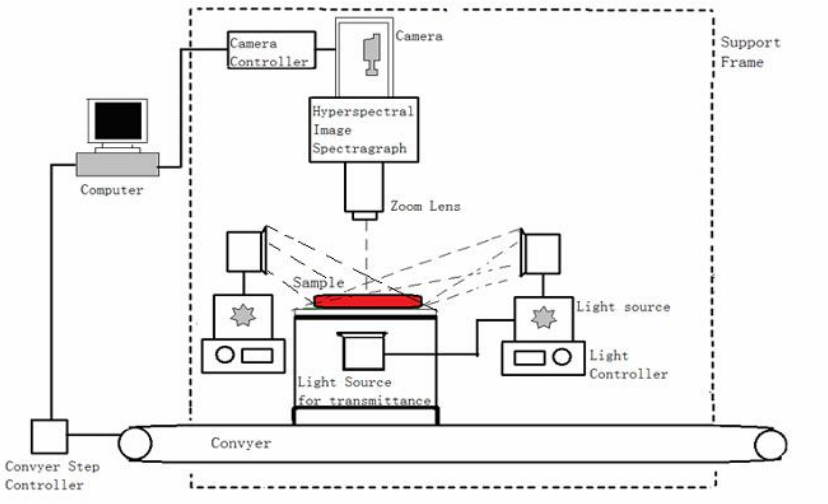

Figure 12: Architecture for applications in machine vision

HSI for microbe detection in food processing

A particular class of food processing problems is the detection of microbes for safety purposes. Table 3 provides an overview of various applications of HSI in this area.

Table 3: HSI for microbial detection and classification

Imaging modality	Sample	Spectral range (nm)	Classification	Type of Microbe detection
Vis–vNIR reflectance	Spinach	400-1000	PCA & ANN	Escherichia coli
Vis–vNIR reflectance	Mushrooms	400-1000	PLS-DA	Pseudomonas tolaasii
Vis–vNIR reflectance	Mandarins	320-1100	CART	Penicillum digitatum
Vis–vNIR reflectance	Pork	400-1100	MLR	Escherichia coli
Vis–vNIR reflectance	Beef	400-1100	MLR	Total viable counts
Vis–vNIR reflectance	Beef	405-970	PLSR	TVC, Pseudomonas spp., and Brochothrix thermosphacta
Vis–vNIR reflectance	Chicken	400-1000	Wavelength band ratio	Fecal material and ingesta
Vis–vNIR reflectance	Maize kernels	400-1000	PCA & DA	Aspergillus
Vis–vNIR	Chicken	400-1000	PLSR	TVC

reflectance				
Vis–vNIR reflectance	Rainbow agar	400-1000	Distance classifier	Escherichia coli
Vis–vNIR reflectance	Rainbow agar	400-1000	PCA & kNN	Escherichia coli
Vis–vNIR reflectance	Blood agar or Campy- Cefex agar	400-1000	PCA & Distance classifier	Campylobacter
Vis–vNIR reflectance	Blood agar or Campy- Cefex agar	400-1000	MLC	Campylobacter
Vis–NIR reflectance	Salmon	400–1700	LS-SVM	TVC
NIR reflectance	pork meat	900-1700	PLSR	TVC
NIR reflectance	Chicken	900-1700	PLSR	Fusarium, Enterobacteriacea, Pseudomonas, TVC
Raman scattering	Water	2857–14285	PCA	Staphylococcus epidermidis
Raman scattering		5714–20000	PCA	Bacillus thuringiensis vegetative cells, Bacillus anthracis spores
Raman scattering		2857–20000	PCA	Bacillus atrophaeus, B. thuringiensis, E. coli, Yersinia rhodei, Yersinia enterocolitica

HSI for fruit and vegetable quality assessment

This section provides a small overview concerning state-of-the-art applications of HSI systems on fruit and vegetable quality evaluation [RD 26]. Quality assessment is highly correlated with the appearance of the product, and is one of the most significant objectives of food quality monitoring. The quality of a particular fruit or vegetable is defined by a set of characteristics, such as color, size, weight, texture, hardness, sweetness, etc., that make it more or less attractive to the consumer. The main goal of an HSI system in food industry is to provide a far more extensive source of information, in order to maximize the quality of each product. Table 4 outlines related work where statistical learning approaches, such as PCA (Principal component analysis), ANN (Artificial neural networks), PLS (Partial least square), and LDA (Linear discriminant analysis), are employed for the detection and the classification of defects in fruits.

Table 4: Statistical techniques applied on Hyperspectral images for disease detection and classification

Reference	Fruit	Statistical technique	Application
Mehl et al. (*2004*)	Red Delicious, Golden Delicious, Gala, and Fuji apples	PCA	Detection of disease, fungal contamination, bruises and soil contamination
Xing et al. (*2005*)	Golden Delicious apples	PCA	Reduction in the number of hyperspectral bands for bruise detection
Qin and Lu (*2005*)	Cherries	PCA & ANN	Detection of pits
Lefcout et al. (*2006*)	Golden Delicious and Red Delicious apples	PCA	Detection of faeces
Xing et al. (*2007a*)	Golden Delicious and Jonagold apples	PCA	Reduction in the number of hyperspectral bands for bruise detection
Xing et al. (*2007b*)	Golden Delicious and Jonagold apples	PCA & PLS	Stem end/calyx end detection
Gowen et al. (*2008*)	White mushrooms	PCA	Bruise detection
Zhao et al. (*2010*)	Crystal pears	PCA	Bruise detection
Li et al. (*2011*)	Oranges	PCA	Bruise detection
Wang et al. (*2012*)	Onions	PCA	Sour skin damage
ElMasry et al. (*2007*)	Strawberry	PLS	MC, SSC, and acidity (expressed as pH) quality attributes
Polder et al. (*2004*)	Tomatoes	PLS	Constitutive compounds at different ripening stages
Nicolaï et al. (*2006*)	Apples	PLS	Identification of bitter pit lesions
Menesatti et al. (*2009*)	Golden Delicious apples	PLS	Assess starch index
Taghizadeh et al. (*2011b*)	White mushrooms	PLS	enzymatic browning
Polder et al. (*2002*)	Tomatoes	LDA	Compare hyperspectral system to standard RGB for ripeness stages
Al-Mallahi et al. (*2008*)	Potatoes	LDA	Distinguish potato tubers from soil clods
Gómez-Sanchis et al. (*2008b*)	Clemenules mandarins	LDA	Decay

Blasco et al. (*2007*)	Citrus fruits	LDA	Segmentation of visible images
Gowen et al. (*2009a*)	White mushrooms	LDA	Early detection of freeze damage
Qin and Lu (*2005*)	Montmorency tart cherries	ANN	Sort cherries with and without pits
Bennedsen et al. (*2007*)	Golden Delicious apples	ANN	Identification of surface defects
Unay and Gosselin (*2006*)	Jonagold apples	ANN	Pixel-wise segmentation of surface defects
Ariana et al. (*2006*)	Honeycrisp, Redcort and Red Delicious apples	ANN	Distinguish bitter pit, soft scald, black rot, decay and superficial scald defects
ElMasry et al. (*2009*)	Red Delicious apples	ANN	Predict the firmness of the apples

Estimation of external product quality parameters

A highly important feature of the products' quality assessment is the proper evaluation of its external quality. For this purpose, HSI systems are proved to be valuable tools not only for the detection of external defects on the fruits and vegetable surfaces, but also for the classification of different types of defects that cannot be easily detected by the human eye. Table 5 overviews some of the most significant applications concerning the evaluation of the external quality using HYP images.

Table 5: HSI related works concerning the estimation of external quality features of fruits.

Reference	Fruit	Features	Wavelengths (nm)
Lefcout et al. (*2006*)	Apples Golden and Red Delicious	Faeces	465–900
Xing and Baerdemaeker (*2005*)	Apples Jonagold	Bruises	400–1,000
ElMasry et al. (*2008b*)	Apples McIntosh	Bruises	400–1,000
Lu (*2003*)	Apples Red Delicious and Golden Delicious	Bruises	900–1,700
Mehl et al. (*2004*)	Apples Red Delicious, Golden Delicious, Gala, and Fuji	Side rots, bruises, flyspecks, scabs, moulds, fungal diseases and soil contaminations	430–900
Karimi et al. (2009)	Avocados	Reflectance	350–2,500

Sugiyama et al. (2010)	Blueberries	Foreign material	1,000–1,600
Gómez-Sanchis et al. (2008b)	Citrus fruits	Decay	460–1,020
Cheng et al. (2004)	Cucumbers	Chilling injury	447–951
Liu et al. (2006)	Cucumbers	Chilling injury	447–951
Qin et al. (2009)	Grapefruits Ruby Red	Canker lesions, greasy spot, insect damage, melanose, scab and wind scarring	450–930
Wang et al. (2011a)	Jujubes	Insect damage	400–720
Wang et al. (2012)	Onions	Sour skin damages	950–1,650
Martinez and Kak (2004)	Oranges	Skin defects	400–720
Qin et al. (2012)	Oranges	Canker lesions, thrips scarring, copper burn, insect damage heterochromatic stripe, scale infestation, phytotoxicity, and wind scarring.	400–1,000
Blasco et al. (2009)	Oranges and mandarins	Thrips scarring, phytotoxicity, wind scarring, scale infestation, chilling injury, sooty mould, oleocellosis, anthracnose, stem-end injury, medfly egg deposition and green mould	Visible, NIR
Zhao et al. (2010)	Pears	Bruises	408–1,117
Gowen et al. (2008)	White mushrooms	Bruises	400–1,000
Gowen et al. (2009a)	White mushrooms	Freeze damage	400–1,000

Estimation of internal quality parameters

HYP imaging systems are able to efficiently quantify the internal quality characteristics of fruits and vegetables, including the flesh and skin color, the firmness, the sugar levels, etc. Table 6 provides an overview of the most representative approaches of HSI based estimation of the internal quality of fruits, adapted from [RD 26].

Table 6: Related works for the estimation of internal quality features of fruits

Reference	Fruit	Features	Wavelengths (nm)
Peirs et al. (*2003*)	Apples	Starch distribution and index	868–1,789
Zhao et al. (*2009*)	Apples Fuji	Sugar content	408–1,117
Menesatti et al. (*2009*)	Apples Golden Delicious	Starch	1,000–1,700
Noh and Lu (*2007*)	Apples Golden Delicious	Flesh and skin colour, firmness, SSC and TA	500–1,000
Noh et al. (*2007*)	Apples Golden Delicious	Flesh and skin colour, firmness, SSC, starch and TA	500–1,000
Mendoza et al. (*2011*)	Apples Golden Delicious Red delicious and Jonagold	Firmness and SSC	500–1,000
ElMasry et al. (*2009*)	Apples Red Delicious	Chilling injury, firmness	400–1,000 nm
Peng and Lu (*2005*)	Apples Red Delicious	Firmness	680, 880, 905, 940
Peng and Lu (*2006*)	Apples Red Delicious and Golden Delicious	Firmness	650–1,000
Rajkumar et al. (*2012*)	Banana	MC, SSC and firmness	400–1,000
Fernandes et al. (*2011*)	Grapes	Anthocyanin concentration	400–1,000
Ariana and Lu (*2010b*)	Pickles	Bloated	675–1,000
ElMasry et al. (*2007*)	Strawberries	MC, SSC and acidity	400–1,000
Qin and Lu (*2005*)	Tart cherries	Pits	400–1,000

2.3.3. Hyperspectral imaging in medical applications

Over the last decades, medical diagnosis has been greatly enhanced by the use of imaging systems, such as magnetic resonance imaging (MRI), computed tomography, ultrasonography, etc. Unlike traditional imaging architectures which are limited to spatial information, HSI has been recently introduced as a powerful medical imaging modality which captures both spatial and spectral content. As a result, HSI provides

valuable information about the physiology, the morphology and the composition of organs and tissues. HSI systems have been shown to be very promising in the fields of medical diagnosis [RD 07, RD 08, RD 09, RD 10], illness prevention [RD 07], disease detection [RD 07, RD 11, RD 13], and image-guided surgery [RD 13]. The following paragraphs overview state-of-the-art applications of HSI systems in the medical field.

Medical Diagnosis

In [RD 07] multiple medical applications of the HSI systems are discussed, in order to prevent or early detect a disease. HSI technology is able to aid in the diagnosis of the cervical (also known as Cervical Intraepithelial Neoplasia-CIN) and the breast cancer.

- **Cancer detection**
  - *Cervical Cancer (CIN)*
    Spectral images can reveal the increased vascularity in subsurface vessels of the cervix that contain hemoglobin, often found in cases of cervical cancer. Another abnormality associated with cervix cancer is the scattering of abnormal cells in the epithelium. The authors in [RD 08] suggested that if spectra can be obtained at multiple wavelengths, then it is possible to discriminate between normal and pre-cancer cervix.
  - Breast Cancer
    While traditional mammographies utilize X-rays to visualize the internal structure of the breast, HSI systems are able to reveal information about molecular properties of precancerous cells (e.g., increased blood and heat in the region of interest).
- **Retinal imaging**
  Most common retinal diseases usually occur above or below the absorbing melanin layer. For this purpose, HSI of the retinal region could be a promising diagnostic tool in revealing abnormalities, such as unbalanced melanin or hemoglobin concentration
- **Tissue characterization**
  Oximetry is the procedure that estimates blood flow perfusion, monitoring the visible and near-infrared spectral properties of blood, recording variation in the percentages of oxygen saturation of hemoglobin. However, oximetry measures the properties of blood only on specific sample points. To overcome these discrepancies, HYP systems can capture the whole body tissue and reveal significant details concerning blood's perfusion that are necessary during a surgery or during the diagnostic procedures. HSI can distinguish a healthy tissue perfusion from an ischemic one.

Dermatology

Another valuable application of HYP imaging can be found in the dermatological evaluation and diagnosis. The authors in [RD 09] propose an effective and automatic method to determine the amount of melanin and hemoglobin in selected areas of the

hand's skin using HYP imaging technology. In this case, the HSI acquisition process implemented using the Specim PFD-V10E[4] camera and the acquired images depict the region of the right hand using two Fitzpatrick skin phototypes. The frequency λ of the data ranges between [397, 1030] nm, while each image is recorded every 0.79 nm, resulting in 800 2D images for each patient, and the spatial resolution of the 2D images is 899 x 1312 pixels.

The automatic extraction of the individual regions of the hand leads to further analysis of the brightness for the specific wavelengths λ. For the case of melanin detection, the frequency ranges between [450, 600] nm while for the case of hemoglobin, the frequency emission ranges between [397, 500] nm. The advantages of the proposed scheme include the automatic comparison of the results of any area of the finger with other areas of the same person, for monitoring of treatment purposes.

2.3.4. Hyperspectral microscopy

Multi and hyperspectral imaging have been recently investigated in the context of optical microscopy in biological imaging applications. Hyperspectral microscopy is an imaging modality which can acquire a sample's full spectroscopic information. It is a functional combination of a traditional high-resolution microscope and spectrometer. The motivation behind developing HM for biomedical applications comes from interest in the biological sample's emission or reflectance spectrum, which contains important structural, biochemical, and physiological information. The observations can be made either at the cellular level, e.g. for the discrimination of spectrally overlapped fluorophores or at the tissue level, e.g. in vivo clinical diagnostics.

Applications

- separation of fluorescence emission signals from multiple fluorophores
- separation of fluorescent label and autofluorescence emission signals
- in-vivo imaging
- FRET analysis

Architectures

- widefield fluorescence microscopy
- confocal microscopy
- in-vivo fluorescence imaging

In order to obtain a better understanding of the applications of HSI in terrestrial applications, Table 7 is adapted from [RD 25] and shows some selected spectral imaging systems used in the biomedical/microscopy field. The key components of the architecture are presented in the Optical Instrument column which describes where one can observe that different architectures employ different combinations of optical

[4] http://www.specim.fi/files/pdf/core/datasheets/PFD_Spectral_Camera-v1-14.pdf

modules such as lens, grating, beamsplitters, colour filter wheels, liquid crystal tuneable filters (LCTF), accoustoptical tuneable filters (AOTF), and sensors as microscopes, spectrographs, endocsopes, and fundus cameras. The key parameters that dictate the performance of each architecture are: the acquisition mode, which includes pushbroom (P), spectral scan (S) and Snapshot Video (V), the spectral range, the Full Width Half Max (FWHM), the spatial resolution and the acquisition time.

Table 7: Current biomedical spectral imaging systems.

Imager	Optical Inst/nt	Mode	Det/or	range (nm)	FWHM (nm)	Spatial res/tion	Acq/ition time	App/tions
Fluorescene imager	Lens & Grating	P	512x512 or 2048x506 CCD	400-1000	0.6-2	9-12 μm		Mouse tumor tissue
Microarray	Lens & Grating	P	576x288 DV465	400-900	3	10-30 μm	5μs	Microarray DNA
Micro/py	Micro & Coded aparture	P	S.B Instrument ST-7XME CCD array	550-665	1	1.54-7.7 μm		Quantum dots
HadamardMicroscopy	Fluorescence Micro/py & Grating	P	512 × 122 CCD	580-745	0.3			Breast tumor and quantum dots
SPLE	Colposcope & Prism	P	Mono/me CCD	400-800	12-28			Stained cervical biopsies sections
HSI tongue	Lens & spectrograph	P	652 × 499 CCD	400-800	5			Tongue, optic nerve head
Fluorescene Micro/py	Micro/pe & spectrograph	P	1536x1024 CCD	380-780	2	0.18 μm	340 msec/line	Human heart, artery section

MPHI	Micro/pe & spectrogh	P	460x300 CCD	400-800	2	1.125 μm		Retina sections, oral cancer cell
MACROscope	Micro/pe & Prism	W	CCD	387-707 / 550-700	6	2 mm	90 s	Colon cancer, tongue, epithelium
NIRSI	Micro/pe & LCTF	S	512x512 CCD	400-720/ 650-1050/ 960-1700	5-10	0.2 mm	536.8 ms/band	Skin, heart, stained tumor sections, blood in tube
In-vivo imager	Lens & LCTF	S	768x512 CCD	420-750	6.8	0.45 mm	50 ms/band	Skin
Active DLP HSI	Lens & DLP Grating	S	1392x1040 CCD	380-780	5	0.13-0.36 mm	11.32 ms /line	Ischemic changes
Multispectral Imager	Lens & LCTF	S	CCD	400-1000	3		40 ms/band	Cervix, Skin
Endoscopic imager	Endos/pe & AOTF	S	512x512 CCD	400-700	1-4			Skin, Brain, tissues
Video Endoscope imager	Endos/pe & AOTF	S	1004x1002 ICCD	400-650	5			Surgery
HSI microscope	Micros/pe & LCTF	S	CCD	400-720	10			Live-viable versus white blood cell, skin
AOTF microscope	Micros/pe & LCTF	S	1317x1035 CCD	450-750		0.36 μm		Binucleated Swiss 3T3 cell, brain

Fourier Spectrometer	Inter/ter Flu/cence Micr/pe	S	100x100 CCD	400-800	4-16	30 µm	5-50 s	Fluor/nce, skin, karyotyping
MSIS	Filter wheel & Lens	S	CCD/InGaAs sensor	R,G,B NIR				Skin, ovary, tooth
Fundus Camera	LCTF & fundus camera	S	CCD	500-650	2		10-15 min	Retina
IRIS	Beam/tter & fundus camera	V	CCD	575-615				
CTIS		V	CCD	450-750	10	1µm		RIN cells
ISS		V	4096x4096 CCD	450-650	5.6 nm	0.45 µm		Fluorescent beads

In addition to the architectures presented in the previous table, Table 8 presents some examples of commercially available HSI systems focused on microscopy.

Table 8: Example of commercial HSI based imaging systems

Product	**Man/turer**	**Optical elements**	**Mode**	**Spectral Range (nm)**	**FWHM (nm)**	**Application**
C1si Spectral Imaging Micro/pe	Nikon	Grating	W	400-750	2.5/5/10	Fluorescence photons, fluorescence redistribution after photobleaching (FRAP) observation
LSM series	Carl Zeis	Array	W	Selectable	1	Multiple fluorescence, live cell imaging, FRAP, fluorescence lose in photobleaching
CytoViva	CytoViva	Grating	P	400-1000	2.8	Drug delivery,

® System						toxicology, fluorescent in live cells
710VP Imager	Surface optics	Grating	P	400-1000	4.7	Biological analysis
PARISS® System	LightForm	Prism	P	365-920	1	Histology, histopathology, CFP/YFP FRE, fluorescent
Benchtop Scanning System	Resonon	Prism	P	400-1000	2.4	Pharma, ischemic wounds, multiple dyes identification
HSi-300/HSI-440C	Gooch & Housego	AOTF	S	450-800	1.5-3	Immunohistochemistry, QDs, FISH, FRET, SKY
Nuance™/ Vectra™ System	CRI	LCTF	S	420-720, 450-950	3-10	In vivo fluorescence, QDs, overstained specimens
IRIS™ retinal imaging system/IMA™	Photon etc	Grating	S	400-1000	2	Retina, dermatology, mapping of copper indium gallium selenide solar cells
DySIS™ Imager	DySISmedical	VIF	S	400-1000	7.5	Cervix diseases detection
SpectraCube system	ASI inc	Interferoemter	V	400-1000	5-20	Karyotyping, fluorescence, skin, cells, tissues
VNIR-20/ VNIR-90 hyperspectral imager	Bodkin design	Hyperpixel ™		450-675, 500-910	11	Retinal imaging, colonoscopy, and skin cancer detection

2.3.5. Hyperspectral imaging in forensics

Spectral imaging techniques have also found a widespread use in the conservation of art and historic objects, such as paintings and documents. Nowadays, HSI systems are widely utilized for the estimation of ink age in historical documents, and for the detection of different hand-writing documents [RD 13]. In [RD 17], the authors present

an overview of HYP techniques along with their applications in conservation of old documents, historical forensic research, biological and environmental monitoring.

HSI systems are critical tools in ink mismatch detection, identifying whether a particular handwritten document was written with a specific pen, or reviling the regions that were written with different pens. An interesting study concerning ink mismatch detection was presented in [RD 14], where the authors developed a HYP database of handwritten notes with multiple black and blue inks. Regardless of the handwriting, they are based on the assumption that same inks present same spectral signatures, while different inks exhibit dissimilarities in their spectral signatures. The following image outlines the aforementioned, presenting the HYP images of different writing inks.

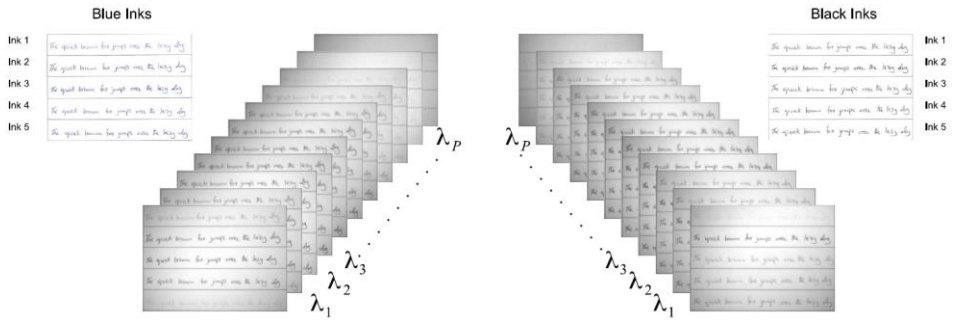

Figure 13: Application in ink detection

Acquisition Process

The authors utilize a camera-captured imaging system, consisting of a monochromatic visual camera, with 752 x 480 pixels spatial resolution. The focusing lens is followed by a Liquid Crystal Tunable Filter (LCTF), in the range of 400 – 720 nm. The target is captured in the visible range, resulting in a 33-bands hyperspectral image.

Main Algorithm

The detection of the different inks is a two-step procedure, including segmentation and clustering of the ink pixels. Given a HSI image, the authors compute a binary mask in order to separate the foreground from the background, using a local threshold based binarization method. The foreground is denoted as the hand-written area, while the background is the blank paper area. Concerning the class assignment of the similar spectral responses, the authors utilize the K-means unsupervised clustering algorithm. In the following plot, the authors present the average normalized spectrum of all blue and black inks respectively. The main conclusion is that the spectra of the inks are distinguished at different ranges in the visible spectrum.

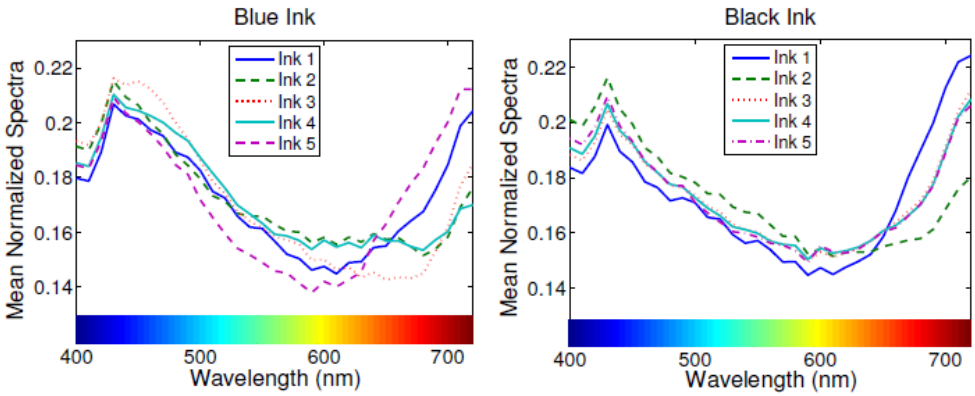

Figure 14: Spectral profile of different inks

Criminology

In criminology, the accurate estimation of the time of the bleeding can provide critical insights. Recently, the authors in [RD 15] proposed an efficient HYP imaging technique that can accurately estimate the age of blood stains that are present in a crime scene and determine whether these blood stains have originated from the same or from different events. When blood exits human body, oxyhemoglobin auto-oxidizes into methemoglobin, which is transformed into hemicrome. As a result, HYP images of the blood stains correspond to a mixture of oxyhemoglobin, methemoglobin and hemicrome. The ratios of these compounds can be directly used in the estimation of blood stain age, up to 200 days old.

Acquisition Process & Analysis

The following image depicts a hypercube of a simulated crime scene, including two spatial and one spectral dimension, presenting also the separation between old and fresh blood stains.

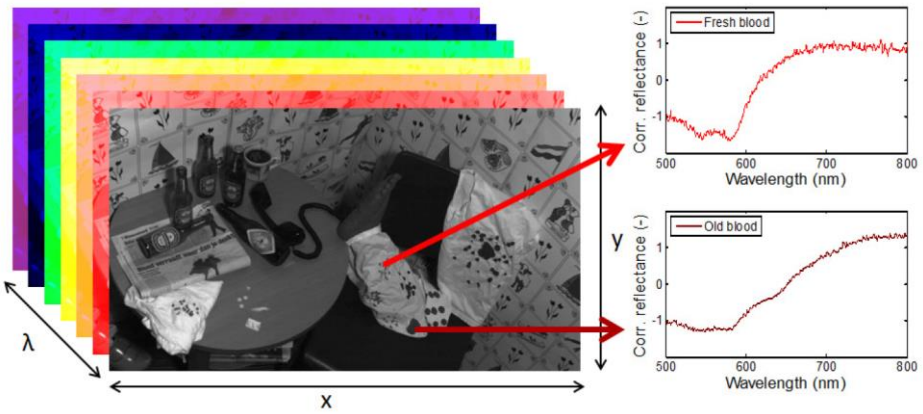

Figure 15: Application of HSI in criminal investigation

In this study, a pushbroom, line-scanning imaging system, is utilized, which consists of a rotary stage, a HSI camera with range between [400, 1000] nm and a halogen broadband white light source. Due to the low camera sensitivity, the spectral analysis wavelength was limited between [500, 800] nm.

2.3.6. Snapshot hyperspectral video imaging

In contrast to state-of-the-art HSI where a repetitive process is employed in order to acquire the full spatio-spectral profile of a scene, Snapshot (or Simultaneous) Spectral Imaging (SSI) systems acquire the complete spatio-spectral cube from a single or a few captured frames, i.e., during a single or a few integration periods, without the need for successive frame acquisition. A consequence of the development of SSI architecture is the capability of recording HYP data in video rates, i.e., from a few to a few hundreds spatio-spectral hypercubes per second. SSI has a huge potential for imaging transient and dynamic events, a situation typical in various applications such a biological imaging and surveillance [RD 23].

One illustrative application of SSI is the analysis and tracking of gas plums where the diffusive nature of the phenomena mandate the acquisition of high frame rate HYP cubes. Another situation where the potentials of HYP video have been explored is in medical imaging, and more specifically, in endoscopy. Similar to the gas plum tracking, the relative motion between the patient and the camera necessitate the acquisition of video HYP imagery at more than 5 c.p.s for in-vivo applications [RD 24]. In addition to scientific imaging, video based HSI has been recently explored in the context of surveillance, where it was observed that one could achieve a significantly more robust tracking by employing spectral information, especially under challenging illumination conditions.

The potential to acquire the full spectral profile of highly dynamic and fast changing processes has a rich potential in biological imaging. Indeed, HSI has been investigated very recently as a tool for *in vitro* retinal oximetry. Figure 16 presents three images of blood cells at different saturation levels associated with different sampling instance (ref. (a)), along with inhogenetities of individual red-cells with respect to deoxygenation (spatial resolution 0.3μm).

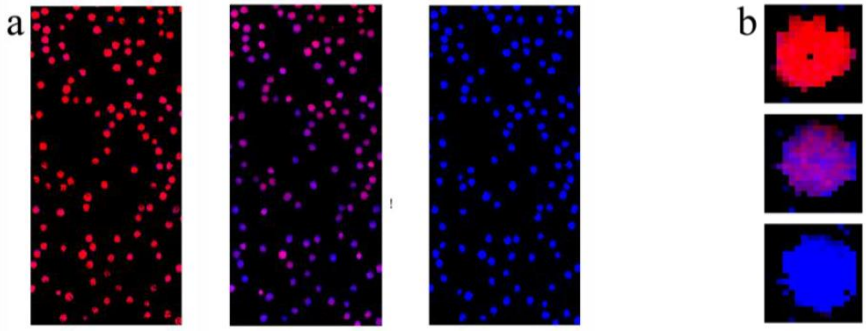

Figure 16: Spectral profiles of red cells during deoxygenation

3. Discussion

The application scenarios presented in the previous sections dictate the key constraints and specification for which the PHySIS system requirements have to be designed on. The scenarios description addressed application needs, operational constraints, technical issues, allowing for the identification of the design parameters that play key roles in the overall performance of the system as a whole.

As already discussed, two main classes of scenarios have been considered: as next steps, all the points common to the individual scenarios will be articulated and collected among the consortium members, and then, according to feedbacks, a more detailed description of the most interesting in each class will be provided. The detailed descriptions will lead to the identification of drivers and requirements and so provide the basis for system design definition (together with its quality verification approach). Design definition itself will follow an iterative development: so both the scenarios and consequently the requirements will be updated as needed during project evolution and adapted according to the results progressively achieved within each specific activity. The first version of the PHySIS scenario descriptions and system requirements will be presented in Deliverable D2.2 due at the end of M3 of the project. In there, we will develop the details of the targeted scenarios, the associated requirements, and the PHySIS system architecture.